RSC Advances

PAPER

Cite this: *RSC Adv.*, 2024, **14**, 22359

Acetate-assisted *in situ* electrodeposited β-MnO_2 for the fabrication of nano-architectonics for non-enzymatic glucose detection

Tianbao Ren, *[a] Lijun Yan[b] and Yang Zhao*[c]

Highly sensitive and low-cost electrocatalytic materials are of great importance for the commercial application of non-enzymatic glucose sensors. Herein, we fabricated a novel one-pot enzyme- and indicator-free method for the colorimetric sensing of blood glucose levels based on the direct redox reaction of β-MnO_2/glucose. Owing to the introduction of ammonium acetate and the enhanced oxygen evolution reaction, the higher conductive β-MnO_2 nanosheets with the larger surface area were directly grown *in situ* on the conductive substrate by a linear sweep voltammetry (LSV) electrodeposition method. Besides, owing to the unique tunnel-type pyrolusite MnO_2, the electrolyte diffusion was facilitated and reduced the response time in the glucose detection process. Hence, the acetate-assisted MnO_2 electrode exhibited a high sensitivity of 461.87 μA M^{-1} cm^{-2} toward glucose, a wide detection range from 1.0 μM to 1 mM, and a low detection limit of 0.47 μM while the electrode also maintained excellent selectivity and stability. These results clearly indicate that the new strategy we developed has great potential for practical applications.

Received 28th May 2024
Accepted 29th June 2024

DOI: 10.1039/d4ra03930k

rsc.li/rsc-advances

1. Introduction

Based on the World Health Organization report, diabetes and its complications are becoming the most dangerous chronic disease caused by the high glucose concentration in human blood and has resulted in approximately 350 million people around the world, and it will be the 7th leading cause of death by 2030 from the current projections.[1–3] Besides, the added sugar in food or drinks is transformed into glucose and eventually into fat in the human body, causing obesity with the modern lifestyle.[4,5] Therefore, with the rapid developments of electrochemical science and technology, the exploitation of the rapid and accurate glucose sensor is a prerequisite for the detection of non-enzymatic material.

In recent years, transition metallic oxides have been widely investigated and used as active materials in non-enzymatic glucose sensors owing to their non-toxic nature, good biocompatibility, boundary active sites, and environmental friendliness.[6–8] Among them, manganese dioxides (MnO_2) exhibit admirable oxidation activity and have drawn the greatest interest in the fields of batteries, supercapacitors, catalysis, or seniors.[9–13] For example, Zhang *et al.* reported a one-pot enzyme- and indicator-free synthesized MnO_2 for the colorimetric sensor.[14] The as-obtained MnO_2 nanomaterial acts as an active nano-oxidizer and a color nano-indicator for the sensing of blood glucose levels. Kovalyk *et al.* electrodeposited MnO_2 on the indium tin oxide substructure with surface decoration to improve operational stability.[15] Various polymorphs of MnO_2 are found due to the different linkages of MnO_6 octahedron units, including α-, β-, γ-, λ-, and δ-types. The α-type has been primarily studied for glucose sensing because of its unique 2 × 2 and 1 × 1 tunnels, which promote electrode kinetics.[16,17] In contrast, despite β-MnO_2 being widely discussed as a material for Li-ion batteries[18,19] or supercapacitors[20,21] due to its high specific capacity, its use as an active material for glucose sensors has been reported in a few studies.

In addition, the sensor electrode can be synthesized with appropriate nanostructures such as nanosheets, nanosphere, nanorods, or nanowires, which is an effective strategy to improve the electro-catalytic property of the active materials. Such a well-designed nanostructure with a large surface area can provide more active sites to participate in the glucose redox reaction and build suitable ion intercalation channels to accelerate the fast electron transfer with a faster current response.[22,23] The considerable nanostructure could be constructed using different methods such as hydrothermal,[24,25] atomic layer deposition,[26] spray pyrolysis,[27] and wet chemical techniques.[28] However, the above-mentioned methods generally require huge energy, special conditions, or complex multistep procedures. In this regard, in order to decrease energy consumption and optimize the fabrication technology, the electrodeposition method has emerged as a competitive

[a]*School of Business, Heze University, Heze 274015*
[b]*Department of Interior and Environmental Design, Pusan National University, Pusan 46241, South Korea*
[c]*Department of Urban and Regional Development, Hanyang University, Seoul 04763, South Korea*

technique to synthesize high-performance electrodes because of its advantages, such as low cost, easy control, faster process, and simplicity.[29,30] Furthermore, according to Donne's theory, the MnO_2 electrodeposition from an aqueous solution occurs by a precipitation reaction within acidic anions formed at the electrode surface.[31] Therefore, the adjusted suitable electrolyte with optimized composition is considered the most important parameter to further improve the electro-catalytic property of the sensor electrode.

Herein, we propose a facile one-step electrodeposition method to fabricate a high-performance β-MnO_2 sensor electrode assisted with ammonium acetate (marked as Ac-MnO_2@NF). In this study, β-MnO_2 was electrodeposited on nickel foam (NF) by the linear sweep voltammetry (LSV) method and served as a detector electrode for glucose sensors. During this process, the introduced ammonium acetate promotes the oxidation of the solvated Mn^{2+} with the occurrence of an oxygen evolution reaction under an applied anodic potential. Accordingly, the morphology of the deposited β-MnO_2 was crystallite growth to a porous nanostructure with a larger surface area and exposed more active sites. Besides, benefits from the unique tunnel-type pyrolusite polymorphs of the as-obtained β-MnO_2, which facilitated the permeation of the electrolyte and shortened the ions transfer distance. Based on the aforementioned synergistic effect, the as-synthesized senor electrode exhibited a wide detection range, low detection limit, excellent stability, and high selectivity in the detection of glucose. This paper provides a new strategy for the design of high-sensitivity sensors concentrating on the prevention and diagnosis of diabetes and its complications.

2. Experimental section

2.1 Synthesis of MnO_2 and Ac-MnO_2 electrodes

MnO_2 and Ac-MnO_2 electrodes were prepared by a facile one-step electrodeposition method. Prior to the electrodeposition, Ni foam with a cross-section of 1×3 cm^2 was ultrasonically cleaned with acetone, 0.1 M HCl solution, alcohol, and deionized water, successively, for 15 min. Then, the experimental procedures were conducted under a three-electrode system, with Ni foam as the working electrode, Pt electrode as the counter electrode, and saturated Ag/AgCl as the reference electrode. MnO_2 was prepared by direct electrodeposition in 0.06 M manganese acetate solution at a potential of 0.6 V for 50 s. Ac-MnO_2 was prepared under the same conditions in a mixed solution of 0.06 M manganese acetate and 0.06 M ammonium acetate. Subsequently, all samples were dried in a vacuum drying oven, and the mass change before and after electrodeposition can be considered the mass of the active substance.

2.2 Materials characterization

The crystalline structure and phase of the products were examined by XRD analysis using a D8 Advance (Germany, Bruker) automated X-ray diffractometer system with Cu-K_α (λ = 1.5 Å) radiation at 40 kV and 40 mA, in the 2θ range of 5° to 60°, at room temperature. The structure and morphology of the samples were characterized *via* field emission scanning electron microscopy (FESEM, JSM-7410F, JEOL, Akishima, Japan) and field emission transmission electron microscopy (FETEM, JEM-2100F, JEOL, Akishima, Japan).

2.3 Electrochemical measurements

Electrochemical experiments were performed in 0.5 M NaOH using a three-electrode electrochemical workstation (RST 5100F). A Pt plate and Ag/AgCl electrode were used as counter and reference electrodes, respectively. CV curves were measured in the potential window of 0–0.6 V at 5, 10, 30, 50, 70, and 100 mV s^{-1}. In electrochemical glucose sensing, the sensing performance of the electrochemical sensor was evaluated using CV and amperometry in 0.1 M NaOH in the absence and presence of glucose.

3. Results and discussion

3.1 Characterization

The schematics for the electrode fabrication are given in Fig. 1. At first, the lattice structure and morphology of the as-formed samples were systematically characterized. Fig. 2a shows the XRD patterns of both MnO_2 electrodes with and without the ammonia treatment. It can be seen that the two samples exhibited similar peaks, which are in agreement with those from the standard cards (JCPDS 80-1098).[32,33] The diffraction peaks at 12.4°, 25.2°, and 37.4° can be indexed to (001), (002), and (111) of the typical δ-MnO_2, respectively. Additionally, based on the Debye–Scherer's equation ($\tau = k\lambda/\beta \cos\theta$), the full width at half maxima (FWHM) of the diffraction peak (002) of Ac-MnO_2 is greater than that of the untreated samples, which indicates the smaller crystallite size and reflects the exposed orientation for β-MnO_2. It can be ascribed to the introduction of ammonium acetate, meaning that the soluble Mn^{3+} intermediate has diffused away from the substrate surface and formed soluble Mn^{2+} and Mn^{4+} by disproportionation.

To further investigate the surface composition and chemical valence of the Ac-MnO_2 sample, X-ray photoelectron spectroscopy (XPS) was performed. The full XPS spectrum showed the presence of Mn 2p and O 1s, where the O 1s peak at 529.88 eV corresponded to the lattice oxygen in the composite and suggested a surface oxidation state upon exposure to air. In the high-resolution spectrum of Mn 2p (Fig. 2c), the peak fitting spectral reveals distinct chemical species, the peaks at 642.04 eV and 654.01 eV corresponded to Mn $2p_{3/2}$ and Mn $2p_{1/2}$, respectively. The spin–orbit level energy spacing was approximately 12 eV, which is consistent with the literature report and indicates the formation of the chemical state of Mn^{2+}.[34,35] The content of Mn^{3+} is relatively low, indicating that the majority of Mn in β-MnO_2 samples exist in the form of +2 valence.[36] These characterization results demonstrated the successful synthesis of the β-MnO_2 sample.

Fig. 3a–d shows the morphology of the various MnO_2 samples by SEM and TEM images. Fig. 2a exhibited a typical nanorod shape with a diameter near 100 nm. As a comparison, Ac-MnO_2 shows a porous nanoflakes morphology and consists

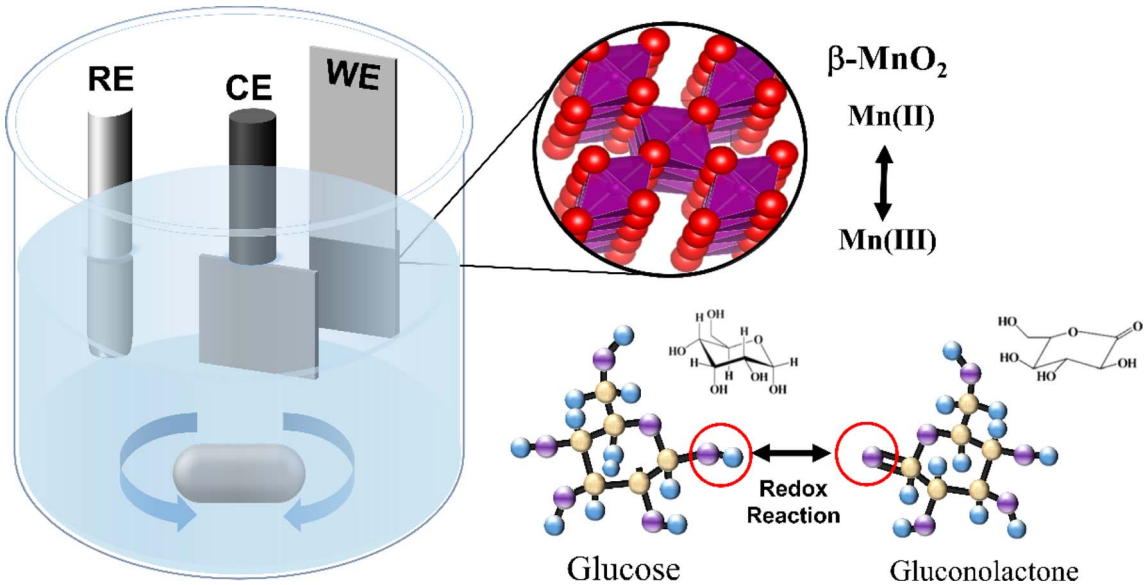

Fig. 1 Schematics of β-MnO_2 electrode fabrication and electrochemical reaction for glucose sensing.

of numerous interconnected nanosheets (as shown in Fig. 2b). After the synchronous progress of electrodeposition and hydrolysis of ammonia acetate, the MnO_2 electrode material ($NH_4^+ : Mn^{2+} = 0.5 : 1$) exhibited a three-dimensional nanosheet structure. Owing to the electrochemical reaction mainly occurring on the surface of the active materials, that larger surface area and 3D porous nanostructure can provide more active sites for the electrochemical reactions and shorten the electron transport path. Such a well-designed nanostructure can be attributed to the hydrolysis of acetate ions, which leads to the improved acidity of the supporting electrolyte and increased conductivity of the electrolyte, which is beneficial to the rapid transfer of Mn^{2+} to form the produced β-MnO_2 with a smaller crystallite size.[37]

Fig. 3c shows the low-resolution TEM image of Ac-MnO_2. As shown, the nanosheets are grown together to form clusters, which correspond to the SEM image. The almost transparent flakes indicate the ultra-thin features, which are favorable for the diffusion of electrolyte ions. The HR-TEM image in Fig. 3d shows the lattice fringes with the inter-planar spacing of about 0.17 nm, which matched the (001) peaks in the XRD pattern.[38] Additionally, the relevant SAED image in the inset shows blurred bright electron diffraction rings, suggesting the amorphous crystal structure of β-MnO_2.

3.2 Electrochemical measurement

Cyclic voltammetry (CV) was applied as the signal transduction mechanism for the determination of the oxidative reactivity of different samples. Fig. 4a and b show the CV curves of the pristine MnO_2 and Ac-MnO_2 electrodes in the 0.5 M NaOH electrolyte at various scan rates. It is well known that electrocatalytic properties, such as oxidation–reduction reactions and fast electron transfer, are essential for the detection of several biomolecules. Hence, a pair of redox peaks appeared in the CV curves of both samples, which correspond to the Mn(IV)/Mn(VI) redox couple. The redox peak current ratio (I_{pa}/I_{pc}) of the MnO_2-based electrodes was close to 1 (1 ≈ reversible), and the well peak-to-peak separation confirmed the reversible redox reaction of glucose–gluconolactone at the interface between active materials and the electrolyte. The obviously enhanced redox

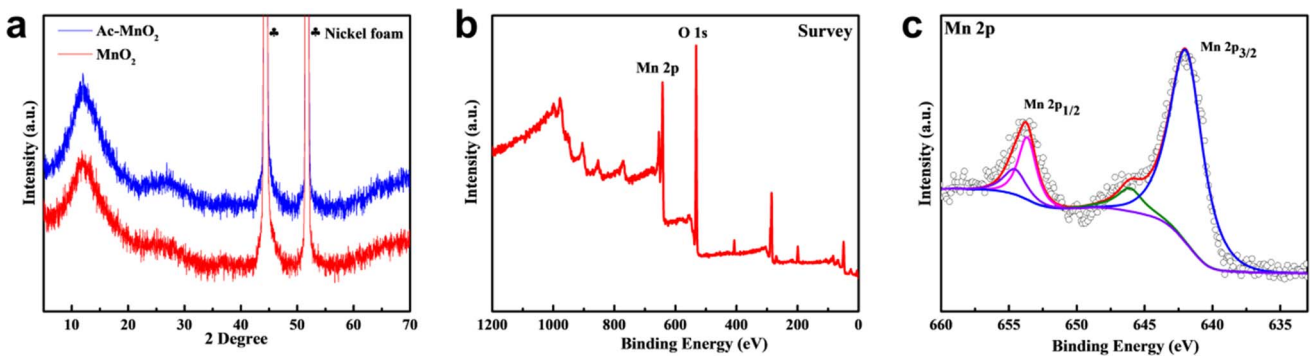

Fig. 2 (a) XRD spectra for the synthesized Ac-MnO_2 and pristine MnO_2 electrode; (b) the XPS survey spectra of β-MnO_2, and (c) Mn 2p spectra.

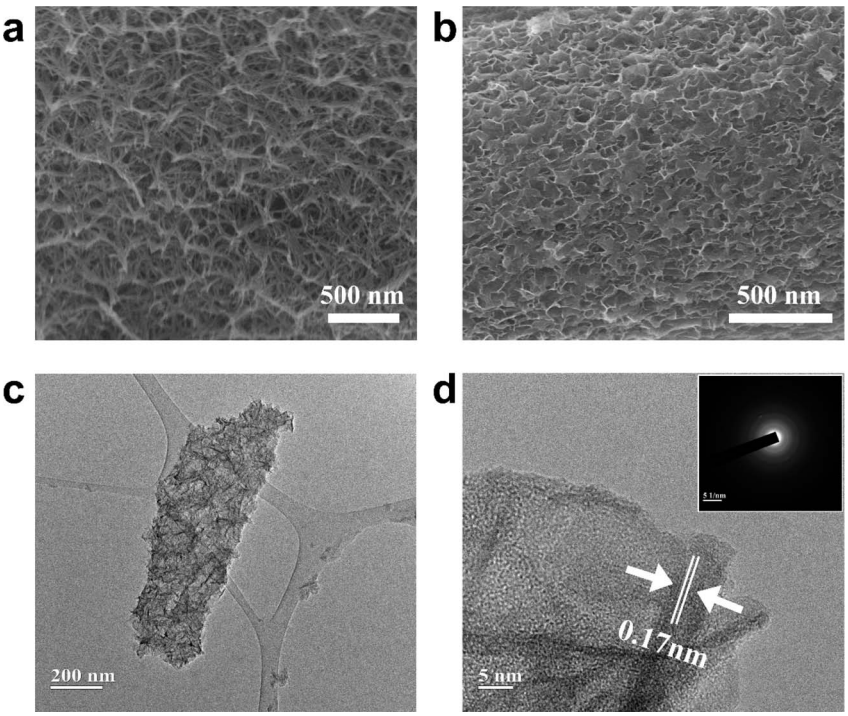

Fig. 3 SEM images of (a) pristine MnO_2 nanosheet; and (b) Ac-MnO_2 nanosheet; TEM (c), HR-TEM (d), and SAED (inset) images of the Ac-MnO_2 nanosheet.

reaction peaks of the Ac-MnO_2 electrode can be ascribed to more active sites that were exposed in the mesoporous nanostructure and enlarged surface area.

The influence of the scan rate on the current response for the anodic and cathodic current was also studied, as shown in Fig. 4c. For the Ac-MnO_2 electrode, the currents of both anodic and cathodic peaks increased with the increase of the square root of the scan rate, and the currents of the two peaks both showed a linear response to the scan rate (ranging from 10 to 100 mV s^{-1}). Such a linear relationship can be obeying from the Randles–Sevcik equation ($i_p = 0.4463n^{3/2}F^{3/2}AD_{app}{}^{1/2}Cv^{1/2}/(RT)^{1/2}$).[39]

By plotting i_p *vs.* $v^{1/2}$, the line regression equations were calculated and shown in the inset of Fig. 4c. The linear relationship between the current response of different MnO_2 electrodes and the square root of the scan rate is proportional to the square root of the scan rates and corresponds to the diffusion-controlled process, that the redox reaction is controlled by the diffusion process of the glucose from the bulk solution/viscous layer interface to the electrolyte/MnO_2 surface interface. However, the linear slope of the pre-treated MnO_2 electrode is obviously higher than that of the pristine MnO_2 electrode. This can be attributed to different material structures and surface oxidation state valences, while the latter limited electrolyte diffusion at high scan speeds and slower charge collection ability.[40] In addition, compared with the pristine MnO_2 electrode, the Ac-MnO_2 electrode showed a significantly improved current response, which can be ascribed to the enlarged surface area with the mesoporous nano-architecture and has shown a good performance to catalyze glucose. Such inferences can also be proven from the amperometric response of the above-mentioned samples with partially increasing glucose concentration in 0.5 M NaOH at a constant applied potential, as shown in Fig. 4d. The steepest slope and higher current density of the Ac-MnO_2 electrode in the fitted straight line, indicate better electrochemical activity related to more exposed active sites.

Despite the treatment, the Ac-MnO_2 electrode shows a higher electro-oxidation ability than the pristine MnO_2 electrode. For amperometric sensing applications, electrodes are generally evaluated by measuring the current response at an optimized potential by adding the analyte.[41] Thus, in order to obtain the best catalytic performance, the amperometric response of the Ac-MnO_2 electrode to gradient addition of various concentrations of glucose in 0.5 M NaOH solution was studied at different voltages. Correspondingly, the results are shown in Fig. 5a, from which it can be seen that the current response at +0.5 V is much higher than that at 0.45 V. Besides, at 0.55 V, unsteady signals were observed due to the excessive background noise. This is because the elevated potentials applied for glucose sensing will trigger the oxidation of electro-active molecules in the system. Accordingly, in order to have a proper signal-to-noise ratio, for obtaining high sensitivity and selectivity, and fast response, and due to the effect of water oxidation at higher potential,[42,43] +0.5 V was chosen as the optimal potential by which the sensor performance was evaluated.

Afterward, the typical amperometric responses with stepwise additions of different concentrations of glucose every 60 seconds are shown in Fig. 5b. The amperometric current responses increased with the gradient concentrations of glucose; it can be seen from the inset that immediately after the

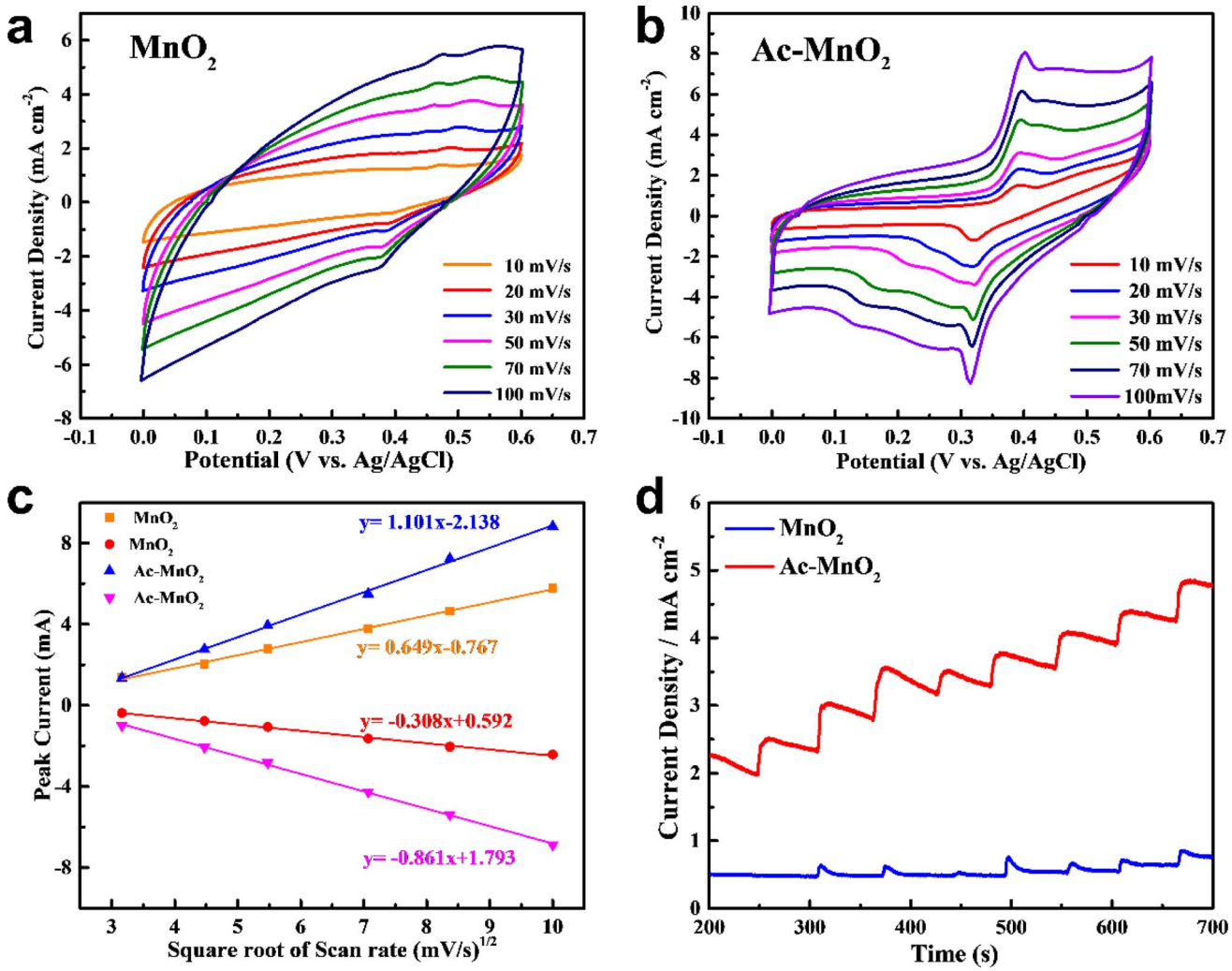

Fig. 4 Cyclic voltammograms of (a) MnO_2 and (b) Ac-MnO_2 electrodes in 0.5 M NaOH at various scan rates. (c) Calibration plot of the peak current *vs.* the square root of scan rates for different samples. (d) Amperometric current, *I* (mA) *vs.* time *T* (s) response of different samples with partially increasing glucose concentration in 0.5 M NaOH at a constant applied potential (*vs.* Ag/AgCl).

addition of glucose, the step-like current response increases rapidly and the steady state was achieved in seconds, indicating that the Ac-MnO_2 electrode effectively catalyzes the oxidation of glucose. According to calculation, the plot of I_{pc} *versus* Ac-MnO_2 provided two linear regression equations as below:

in the range of 1.0 μM to 1 mM, $I\,(\mu A) = 14.6 + 65.75C_{glucose}$, $R^2 = 0.996$; and,

in the range of 1.0 mM to 28 mM, $I\,(\mu A) = 130.6 + 115.75C_{glucose}$, $R^2 = 0.994$.

The calibration plot showed a noticeably low detection limit (LOD: limit of detection) of 0.47 μM (where the ratio of signal-to-noise S/N = 3), and the sensitivity was calculated to be 461.87 μA M^{-1} cm^{-2}. In the linear range of less than 1.0 mM of the fit, the Ac-MnO_2 electrode could ideally absorb the added glucose molecules and desorb the reaction byproducts efficiently to allow further catalytic reactions to take place. Then, the increment of sensing current started to decay above 1.0 mmol L^{-1} glucose concentration, which was a higher concentration; this can be ascribed to the fact that most of the active sites on the electrode were covered by glucose and the current response was reduced, thus decreasing the diffusion coefficient and slowing down the electron transfer.[44,45] In order to evaluate the performance of the as-prepared electrode, the linear range, sensitivity, and limit of detection (LOD) of the Ac-MnO_2 electrode presented in this study are compared to those of other similar MnO_2-based sensors, as summarized in Table 1.

In practical applications, the repeatability, reproducibility, stability, and selectivity, called the anti-interference analysis, of the sensor are of great significance.[50] Some interfering substances such as sodium chloride (NaCl), uric acid (UA), ascorbic acid (AA), dopamine acid (DA), and fructose (Fru) are commonly found in the human body, and the physiological glucose level is normally 10 times higher than the interferences. Thus, we sequentially dropped 0.5 mM glucose, 0.05 mM NaCl, UA, AA, DA, Fru, and 0.5 mM glucose under 0.5 V to compare the sensing ability of the electrodes. Fig. 5c shows the measuring result of the anti-

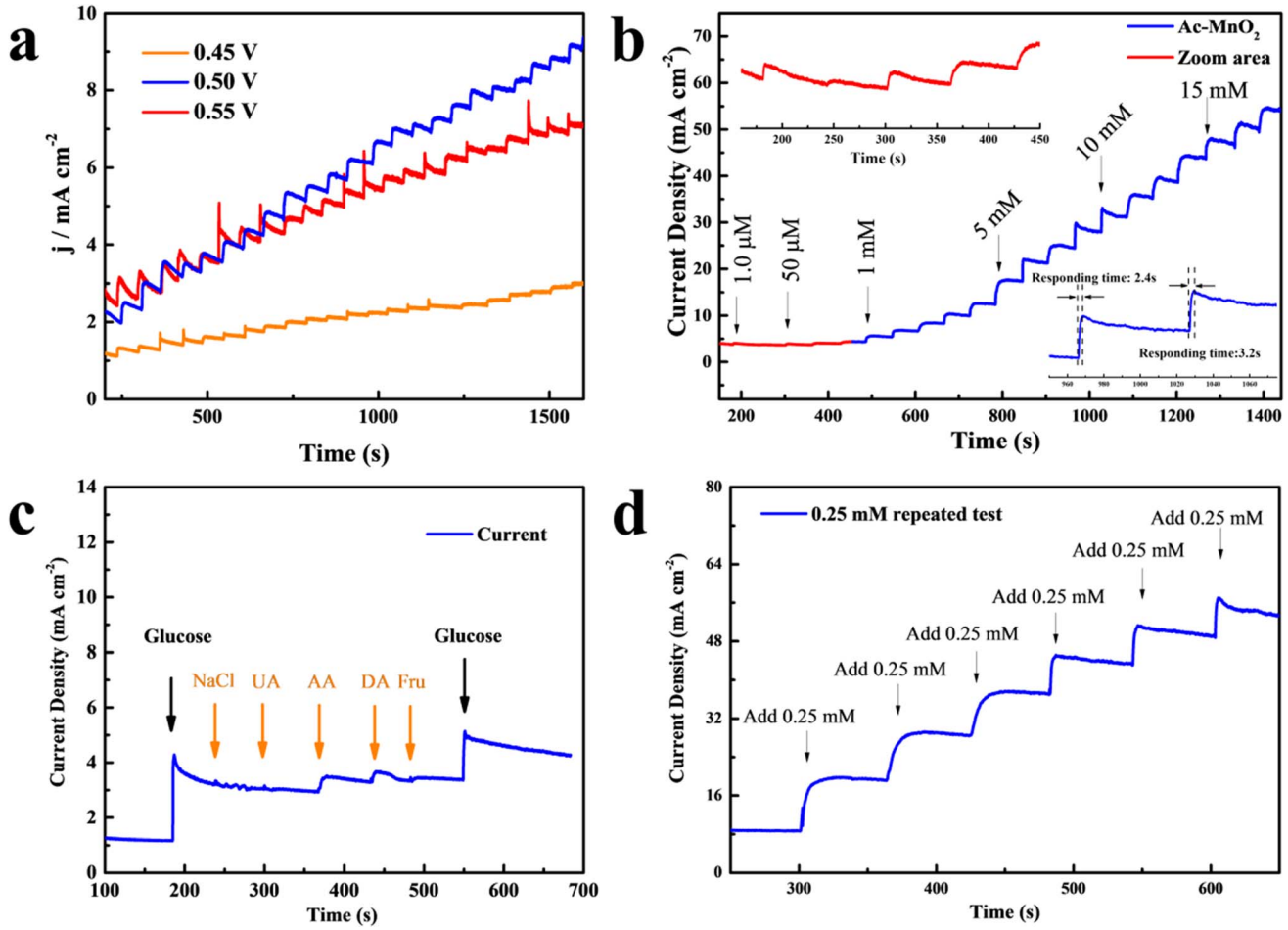

Fig. 5 Amperometric current, I (mA) *vs.* time T (s) response of the Ac-MnO_2 electrode with (a) increasing glucose concentration in 0.5 M NaOH at different applied potentials; (b) against successive additions of different glucose concentrations in 0.5 M NaOH at a constant applied potential of 0.5 V; the inset shows the zoom area of the linear range and the selected response times; (c) the addition of glucose (0.5 mM) and different inferences (0.05 mM) in 0.5 M NaOH at an applied potential of 0.5 V; (d) and the repeatability measurement (*vs.* Ag/AgCl).

interference analysis. The first time added glucose was detected expeditiously as expected. Subsequently, the amperometric responses of NaCl, UA, and Fru were almost invisible. Despite the current responses of AA and DA appearing marginally, such a slight amount is easily distinguished from glucose. Then, the current change after again adding glucose was not affected by the presence of other substances, further, indicating a good selectivity of the constructed sensor. Besides, the repeatability of the same MnO_2 sensor was evaluated through six independent measurements, as shown in Fig. 5d. A smooth and stable current response without any signature deformation was achieved along with the repeat addition of glucose. The CA curve with a low relative standard deviation (RSD) reveals the excellent catalytic ability and stable nanostructure of the active materials.

Table 1 The catalytic performance evaluation of MnO_2-based sensors for the detection of glucose

Electrode materials	Linear range (mM)	Sensitivity ($\mu A\ mM^{-1}\ cm^{-2}$)	Detection limit (LOD; μM)	References
MnO_2	0–0.1		12.8	11
MnO_2/CuNC	0.001–0.2		100	46
MnO_2/Si	0.0001–0.01	918.4	0.39	47
MnO_2/CNT	0.0005–1.0	3406.4	0.5	48
MnO_2/CFF	0.01–4.5	1650.6	1.9	49
MnO_2/MWs	0.01–28	33.19	10	41
Ac-MnO_2@NF	0.001–1.0	461.87	0.47	Our work

4. Conclusions

In summary, a highly sensitive MnO_2 structure was prepared on a 3D porous nickel foam substrate using ammonium acetate assisted by a facile LSV electrodeposition for the electrochemical oxidation application. Hence, compared with the pristine MnO_2 electrode, the introduced acetate ions with a suitable acidic atmosphere converted the morphology of the MnO_2 into an interconnected porous nanosheet with an enlarged surface area. Therefore, the porous nanostructure provides abundant active sites for glucose oxidization and accelerates the excellent electron/ion transfer at the interface between active materials and electrolytes. As a result, the uniformly deposited Ac-MnO_2 electrode exhibited a faster and more remarkable current response towards glucose than the pristine MnO_2 electrode. Meanwhile, it displayed a high sensitivity of 461.87 $\mu A\ M^{-1}\ cm^{-2}$ to glucose, a wide detection range of 1.0 μM to 1 mM, and a low detection limit of 0.47 μM, while the electrode also maintained excellent selectivity and stability. Owing to its excellent catalytic performance, our proposed electrodeposition method establishes a new strategy for the development of MnO_2 nanomaterials with well-designed nanoarchitectonics. This approach represents an attractive strategy for achieving high-sensitivity glucose detection and provides inspiration for a variety of advanced sensors.

Data availability

The datasets generated and/or analyzed during the current study are available from the corresponding author on reasonable request. All data supporting the findings of this study are included in this published article. Any additional datasets used and/or analyzed during the current study are available from the corresponding author upon reasonable request.

Conflicts of interest

There are no conflicts to declare.

References

1 L. F. de Lima, A. d. S. de Freitas, A. L. Ferreira, C. C. Maciel, M. Ferreira and W. R. de Araujo, Enzymeless glucose sensor based on disposable Ecoflex®/graphite thermoplastic composite substrate modified with Au@ GQDs, *Sens. Actuators Rep.*, 2022, **4**, 100102.

2 A. Mohammadpour-Haratbar, S. Mohammadpour-Haratbar, Y. Zare, K. Y. Rhee and S.-J. Park, A Review on Non-Enzymatic Electrochemical Biosensors of Glucose Using Carbon Nanofiber Nanocomposites, *Biosensors*, 2022, **12**(11), 1004.

3 M. Adeel, M. M. Rahman, I. Caligiuri, V. Canzonieri, F. Rizzolio and S. Daniele, Recent advances of electrochemical and optical enzyme-free glucose sensors operating at physiological conditions, *Biosens. Bioelectron.*, 2020, **165**, 112331.

4 Z. Zhao, Q. Li, Y. Sun, C. Zhao, Z. Guo, W. Gong, J. Hu and Y. Chen, Highly sensitive and portable electrochemical detection system based on AuNPs@ CuO NWs/Cu2O/CF hierarchical nanostructures for enzymeless glucose sensing, *Sens. Actuators, B*, 2021, **345**, 130379.

5 A. B. Urgunde, A. R. Kumar, K. P. Shejale, R. K. Sharma and R. Gupta, Metal wire networks functionalized with nickel alkanethiolate for transparent and enzymeless glucose sensors, *ACS Appl. Nano Mater.*, 2018, **1**(10), 5571–5580.

6 Z. Lu, Y. Zhang, M. Sun, P. Zou, X. Wang, Y. Wang, Q. Huang, H. Chen, J. Ye and H. Rao, N-doped carbon dots regulate porous hollow nickel-cobalt sulfide: High-performance electrode materials in supercapacitor and enzymeless glucose sensor, *J. Power Sources*, 2021, **516**, 230685.

7 T. H. Ko, J.-G. Seong, S. Radhakrishnan, C.-S. Kwak, M.-S. Khil, H.-Y. Kim and B.-S. Kim, Dual functional nickel cobalt/MWCNT composite electrode-based electrochemical capacitor and enzymeless glucose biosensor applications: Influence of Ni/Co molar ratio, *J. Ind. Eng. Chem.*, 2019, **73**, 1–7.

8 X. Ma, J. Chen, B. Yuan, Y. Li, L. Yu and W. Zhao, Three-dimensional hollow nickel phosphate microspheres with controllable hoya-like structure for high-performance enzymeless glucose detection and supercapacitor, *Appl. Surf. Sci.*, 2022, **588**, 152928.

9 L. Sinha, S. Pakhira, P. Bhojane, S. Mali, C. K. Hong and P. M. Shirage, Hybridization of Co3O4 and α-MnO2 nanostructures for high-performance nonenzymatic glucose sensing, *ACS Sustain. Chem. Eng.*, 2018, **6**(10), 13248–13261.

10 R. Ponnusamy, A. Gangan, B. Chakraborty, D. J. Late and C. S. Rout, Improved nonenzymatic glucose sensing properties of Pd/MnO2 nanosheets: synthesis by facile microwave-assisted route and theoretical insight from quantum simulations, *J. Phys. Chem. B*, 2018, **122**(31), 7636–7646.

11 Z. Huang, L. Zheng, F. Feng, Y. Chen, Z. Wang, Z. Lin, X. Lin and S. Weng, A simple and effective colorimetric assay for glucose based on MnO2 nanosheets, *Sensors*, 2018, **18**(8), 2525.

12 S. E. Kim, J. C. Yoon, H.-J. Tae and A. Muthurasu, Electrospun Manganese-Based Metal–Organic Frameworks for MnO x Nanostructures Embedded in Carbon Nanofibers as a High-Performance Nonenzymatic Glucose Sensor, *ACS Omega*, 2023, **8**(45), 42689–42698.

13 K. Okamoto, H. Kawakami, Y.-A. Chien, T. Kurioka, W.-T. Chiu, P. Chakraborty, T. Nakamoto, Y.-J. Hsu, M. Sone and T.-F. M. Chang, Gold/MnO2 particles decorated on electrodeposited polyaniline toward non-enzymatic electrochemical sensor for glucose, *Micro Nano Eng.*, 2023, **18**, 100175.

14 J. Zhang, X. Dai, Z.-L. Song, R. Han, L. Ma, G.-C. Fan and X. Luo, One-pot enzyme-and indicator-free colorimetric sensing of glucose based on MnO2 nano-oxidizer, *Sens. Actuators, B*, 2020, **304**, 127304.

15 A. Kovalyk, O. Tananaiko, A. Borets, M. Etienne and A. Walcarius, Voltammetric and microscopic characteristics of MnO2 and silica-MnO2hybrid films

electrodeposited on the surface of planar electrodes, *Electrochim. Acta*, 2019, **306**, 680–687.
16 N. Sohal, B. Maity and S. Basu, Morphology-dependent performance of MnO2 nanostructure–carbon dot-based biosensors for the detection of glutathione, *ACS Appl. Bio Mater.*, 2021, **4**(6), 5158–5168.
17 Z. Wang, J. Bao, J. Du, L. Luo, G. Xiao and T. Zhou, Sulfamethoxazole degradation by alpha-MnO2/periodate oxidative system: role of MnO2 crystalline and reactive oxygen species, *Environ. Sci. Pollut. Res.*, 2022, **29**(29), 44732–44745.
18 L. Li, T. K. Hoang, J. Zhi, M. Han, S. Li and P. Chen, Functioning mechanism of the secondary aqueous Zn-β-MnO2 battery, *ACS Appl. Mater. Interfaces*, 2020, **12**(11), 12834–12846.
19 X. Liao, C. Pan, Y. Pan and C. Yin, Synthesis of three-dimensional β-MnO2/PPy composite for high-performance cathode in zinc-ion batteries, *J. Alloys Compd.*, 2021, **888**, 161619.
20 N. S. Shaikh, S. S. Mali, J. V. Patil, A. I. Mujawar, J. S. Shaikh, S. C. Pathan, S. Praserthdam, C. K. Hong and P. Kanjanaboos, Mg2+ ion-powered hybrid supercapacitor with β-MnO2 as a cathode and α-Fe2O3 as an anode, *J. Energy Storage*, 2022, **50**, 104525.
21 T. Putjuso, S. Putjuso, A. Karaphun, S. Nijpanich, N. Chanlek and E. Swatsitang, Hydrothermally obtained β-MnO2 nanoparticles/activated carbonized coconut fibers composites, electrochemical properties study for future energy storage devices, *Appl. Surf. Sci.*, 2023, **618**, 156653.
22 H. Li, X. Chen, E. Zalnezhad, K. Hui, K. Hui and M. J. Ko, 3D hierarchical transition-metal sulfides deposited on MXene as binder-free electrode for high-performance supercapacitors, *J. Ind. Eng. Chem.*, 2020, **82**, 309–316.
23 H.-W. Chang, C.-L. Dong, Y.-H. Chen, Y.-Z. Xu, T.-C. Huang, S.-C. Chen, F.-J. Liu, Y.-H. Lai and Y.-C. Tsai, Extended Graphite Supported Flower-like MnO2 as Bifunctional Materials for Supercapacitors and Glucose Sensing, *Nanomaterials*, 2021, **11**(11), 2881.
24 R. Ponnusamy, R. Venkatesan, M. Kandasamy, B. Chakraborty and C. S. Rout, MnO2 polymorph selection for non-enzymatic glucose detection: an integrated experimental and density functional theory investigation, *Appl. Surf. Sci.*, 2019, **487**, 1033–1042.
25 A. Umar, A. A. Ibrahim, R. Kumar, H. Albargi, W. Zeng, M. A. M. Alhmami, M. A. Alsaiari and S. Baskoutas, Gas sensor device for high-performance ethanol sensing using α-MnO2 nanoparticles, *Mater. Lett.*, 2021, **286**, 129232.
26 Z. Wei, Z. Hai, M. K. Akbari, D. Qi, K. Xing, Q. Zhao, F. Verpoort, J. Hu, L. Hyde and S. Zhuiykov, Atomic layer deposition-developed two-dimensional α-MoO3 windows excellent hydrogen peroxide electrochemical sensing capabilities, *Sens. Actuators, B*, 2018, **262**, 334–344.
27 M. Zahan and J. Podder, Role of Fe doping on structural and electrical properties of MnO2 nanostructured thin films for glucose sensing performance, *Mater. Sci. Semicond. Process.*, 2020, **117**, 105109.
28 T. Kondo, Y. Matsushima, K. Matsuda and H. Unuma, Amperometric sensing of H2O2 and glucose using wet-chemically deposited MnO2 thin films, *J. Ceram. Soc. Jpn.*, 2018, **126**(4), 260–262.
29 Q. Liu, D. Chen and Z. Kang, One-step electrodeposition process to fabricate corrosion-resistant superhydrophobic surface on magnesium alloy, *ACS Appl. Mater. Interfaces*, 2015, **7**(3), 1859–1867.
30 Z.-M. Huang, Q.-Y. Cai, D.-C. Ding, J. Ge, Y.-L. Hu, J. Yang, L. Zhang and Z.-H. Li, A facile label-free colorimetric method for highly sensitive glutathione detection by using manganese dioxide nanosheets, *Sens. Actuators, B*, 2017, **242**, 355–361.
31 M. F. Dupont and S. W. Donne, Nucleation and growth of electrodeposited manganese dioxide for electrochemical capacitors, *Electrochim. Acta*, 2014, **120**, 219–225.
32 B. Chen, B. Wu, L. Yu, M. Crocker and C. Shi, Investigation into the catalytic roles of various oxygen species over different crystal phases of MnO2 for C6H6 and HCHO oxidation, *ACS Catal.*, 2020, **10**(11), 6176–6187.
33 X. Zhao, Y. Hou, Y. Wang, L. Yang, L. Zhu, R. Cao and Z. Sha, Prepared MnO 2 with different crystal forms as electrode materials for supercapacitors: experimental research from hydrothermal crystallization process to electrochemical performances, *RSC Adv.*, 2017, **7**(64), 40286–40294.
34 Y.-K. Duan, Z.-W. Li, S.-C. Zhang, T. Su, Y.-F. Ma, A.-J. Jiao and Z.-H. Fu, Metal-organic frameworks (MOFs)-derived Mn2SnO4@ C anode based on dual lithium storage mechanism for high-performance lithium-ion capacitors, *Chem. Eng. J.*, 2023, **477**, 146914.
35 C. Zhu, Q. Wu, F. Yuan, J. Liu, D. Wang and Q. Zhang, Novel Electrochemical Sensor Based on MnO2 Nanowire Modified Carbon Paper Electrode for Sensitive Determination of Tetrabromobisphenol A, *Chemosensors*, 2023, **11**(9), 482.
36 P. W. Menezes, A. Indra, V. Gutkin and M. Driess, Boosting electrochemical water oxidation through replacement of O h Co sites in cobalt oxide spinel with manganese, *Chem. Commun.*, 2017, **53**(57), 8018–8021.
37 G. Ashraf, M. Asif, A. Aziz, T. Iftikhar, Z.-T. Zhong, S. Zhang, B. Liu, W. Chen and Y.-D. Zhao, Advancing interfacial properties of carbon cloth via anodic-induced self-assembly of MOFs film integrated with α-MnO2: A sustainable electrocatalyst sensing acetylcholine, *J. Hazard. Mater.*, 2022, **426**, 128133.
38 M.-y. Liang, B. Zhao, Y. Xiong, W.-x. Chen, J.-z. Huo, F. Zhang, L. Wang and Y. Li, A "turn-on" sensor based on MnO 2 coated UCNPs for detection of alkaline phosphatase and ascorbic acid, *Dalton Trans.*, 2019, **48**(43), 16199–16210.
39 L. Chen, X. Huang, X. Zeng, G. Fang, W. Chen, H. Zhou, X. Zhong and H. Cai, Signal-on bimodal sensing glucose based on enzyme product-etching MnO2 nanosheets for detachment of MoS2 quantum dots, *Chin. Chem. Lett.*, 2021, **32**(6), 1967–1971.
40 V. Poltavets, M. Krawczyk, G. Maslak, O. Abraimova and M. Jönsson-Niedziółka, Formation of MnO 2-coated ITO

electrodes with high catalytic activity for enzymatic glucose detection, *Dalton Trans.*, 2023, **52**(38), 13769–13780.

41 J. Chen, W.-D. Zhang and J.-S. Ye, Nonenzymatic electrochemical glucose sensor based on MnO2/MWNTs nanocomposite, *Electrochem. Commun.*, 2008, **10**(9), 1268–1271.

42 J. Zhang, X. Zhu, H. Dong, X. Zhang, W. Wang and Z. Chen, In situ growth cupric oxide nanoparticles on carbon nanofibers for sensitive nonenzymatic sensing of glucose, *Electrochim. Acta*, 2013, **105**, 433–438.

43 Z. Yang and X. Dou, Emerging and future possible strategies for enhancing 1D inorganic nanomaterials-based electrical sensors towards explosives vapors detection, *Adv. Funct. Mater.*, 2016, **26**(15), 2406–2425.

44 Z. Yin, K. Allado, A. T. Sheardy, Z. Ji, D. Arvapalli, M. Liu, P. He, X. Zeng and J. Wei, Mingled MnO2 and Co3O4 Binary nanostructures on well-aligned electrospun carbon nanofibers for nonenzymatic glucose oxidation and sensing, *Cryst. Growth Des.*, 2021, **21**(3), 1527–1539.

45 N. Sohal, B. Maity, N. P. Shetti and S. Basu, Biosensors based on MnO2 nanostructures: A review, *ACS Appl. Nano Mater.*, 2021, **4**(3), 2285–2302.

46 H.-B. Wang, Y. Chen, N. Li and Y.-M. Liu, A fluorescent glucose bioassay based on the hydrogen peroxide-induced decomposition of a quencher system composed of MnO 2 nanosheets and copper nanoclusters, *Microchim. Acta*, 2017, **184**, 515–523.

47 Q. Tan, R. Zhang, R. Kong, W. Kong, W. Zhao and F. Qu, Detection of glutathione based on MnO 2 nanosheet-gated mesoporous silica nanoparticles and target induced release of glucose measured with a portable glucose meter, *Microchim. Acta*, 2018, **185**, 1–7.

48 C. Guo, H. Li, X. Zhang, H. Huo and C. Xu, 3D porous CNT/MnO2 composite electrode for high-performance enzymeless glucose detection and supercapacitor application, *Sens. Actuators, B*, 2015, **206**, 407–414.

49 X. Weina, L. Guanlin, W. Chuanshen, C. Hu and X. Wang, A novel β-MnO2 micro/nanorod arrays directly grown on flexible carbon fiber fabric for high-performance enzymeless glucose sensing, *Electrochim. Acta*, 2017, **225**, 121–128.

50 S.-J. Li, J.-C. Zhang, J. Li, H.-Y. Yang, J.-J. Meng and B. Zhang, A 3D sandwich structured hybrid of gold nanoparticles decorated MnO2/graphene-carbon nanotubes as high performance H2O2 sensors, *Sens. Actuators, B*, 2018, **260**, 1–11.